Goniocolorimetry: from measurement to representation in the CIELAB color space

Lionel Simonot

PHYMAT: Physique des Matériaux, UMR CNRS 6630, Boulevard Marie et Pierre Curie, BP 179, 86962 Futuroscope Chasseneuil Cedex, France

Corresponding author: lionel.simonot@univ-poitiers.fr

Mathieu Hébert

Ecole Polytechnique Fédérale de Lausanne (EPFL), School for Computer and Communication Sciences, 1015 Lausanne, Switzerland

Damien Dupraz

STIL SA, 595 rue Pierre Berthier, Domaine de St Hilaire, F-13855 Aix en Provence Cedex 3, France

Abstract

The classical definitions of color are well adapted to diffusing objects, whose color is almost independent of the viewing angle, and to very glossy object observed in the specular direction in respect to the light source. For glossy or iridescent objects, the color is difficult to characterize due to its dependence on the viewing direction. In order to cope with such objects and to represent their angle-dependent colors in a colorimetric space, we adapt the CIELAB space to “goniocolorimetric” measurements. A crucial point when defining this space is the statement of the viewing solid angle. First, we suggest performing a BRDF measurement at high angular resolution in order to characterize the gloss of the specimen. Then, since for the definition of colors the CIE recommends cones of half-angle of 2° or 10°, we propose to convert the measured BRDF into a reflectance factor defined in respect to these solid angles. This procedure is eased by a planar multispectral image of the BRDF, where solid angles are specified by the pixel size. At last, the reflectance factors are converted into CIELAB coordinates. By using this procedure, the perfect white diffuser but also the perfect mirror can be represented in this colorimetric space.

Keywords

Colorimetry, gloss, geometric aspect, reflectance, spectrophotometry, BRDF

Preprint of article published in Color Research and Application, Vol. 36, Issue 1, Feb 2011, pp. 1-10
© 2011 Wiley Periodicals Inc.

1. Introduction

The visual appearance of objects is a major criterion of acceptability for manufacturers, especially in the domains of printing, automotive, cosmetic, textiles and food. Appearance is usually described according to five distinct factors: form, texture, transparency, gloss and color. These visual attributes are the response by the human visual perception system to the light signal issued from the object after possible complex light-matter interactions.

Color is the visual attribute whose mechanism of perception by the human visual system has been the best characterized, in particular thanks to the works by the Commission Internationale de l'Eclairage (CIE) along the 20th century [1]. Color is related to the spectral distribution of light in the visible wavelength domain, which can be measured using a spectrophotometer. But the stimulated regions in the retina have also an influence in the perception of color. The color science, called colorimetry, has been eased by a mathematical representation where each color is represented by the tristimulus values X, Y and Z defined from the CIE color matching functions of the standard observer [1, 2, 3]. They take into account the differences in color appreciation in terms of the retinal area reached by the light. In 1931, the CIE established the standard observer trichromatic functions for light contained within a cone of 2° half-angle centered on the optical axis. This solid angle was selected to stimulate the foveal area, region of the retina where the cone cells are numerous and the rod cells are almost absent. In order to obtain a better matching between color definitions and the viewing conditions in the everyday life, the CIE defined in 1964 different standard observer color matching functions by considering a larger solid angle, i.e. a cone of 10° half-angle.

In the case of objects, color is related to a spectrum modification, i.e. to a variation of the incident spectrum due to the reflection by the object. Before being interpreted as color, the sensorial response by the retina to the reflected light (tristimulus values X, Y and Z) is combined with other information, especially the response by the retina to the light reflected by a reference diffuser (tristimulus values X_{ref}, Y_{ref} and Z_{ref}). In order to take into account the relative perception mechanism with respect to the illumination source, several color spaces were defined, e.g. the CIELAB coordinate system [1, 2, 3]. Color coordinates are calculated in respect to a standard illuminant whose spectrum is fixed by the CIE.

The angular distribution of the reflected light determines the type of geometry that should be used for measurement, especially the solid angle of detection. When an object is strongly scattering, e.g. a matte paint or paper, its spectrum is almost independent of the incident and viewing directions. Since the detector is filled with the homogenous diffuse light, the quantity of collected light is proportional to the solid angle of the detector. In contrast, when the object is very glossy, e.g. a metallic plate or a dielectric plane surface for optical coating [4], collimated incident light is reflected around a single direction, called the specular direction. If the reflected light pencil is infinitely thin, the size of the detector and its solid angle have no influence on the measurement.

In many cases, the object is neither very scattering nor very glossy but in between [5, 6, 7]. A satin-finish painting, for example, reflects a diffuse colored component issued from the painting itself as well as an uncolored component scattered by the surface. The proportion of these two components varies with the observation direction. Since they are added, the spectrophotometer measures them at the time and cannot distinguish them. However, they are perceived by a human observer as distinct appearance attributes, i.e. as color and gloss. The perception of gloss relies on an analysis of angle-

dependent color variations by the human visual system, which is still a subject of investigation [8, 9, 10].

There exists one special class of objects for which gloss can be easily discarded from color measurements: the objects composed of a diffusing material having a smooth surface. The colored diffuse component is spread rather homogeneously over the hemisphere whereas the gloss is directed only into the specular direction. To measure the color without gloss component, one can use a directional light source and capture light at an angle different from the specular direction, e.g. the 45°:0° geometry recommended by the CIE, where the incident light comes at 45° and the reflected light is detected at 0°. For geometries relying on an integrating sphere, a gloss trap located around the specular direction enables discarding the specular component, e.g. the 8°:de geometry also recommended by the CIE [1]. Many measuring instruments, especially portative spectrophotometers, rely on these geometries and offer the possibility to discard the gloss. In practice, one can consider that gloss is effectively discarded when the material looks sufficiently diffusing and the surface looks sufficiently smooth, which already concerns a wide range of objects (e.g. glossy prints, photographs, ceramics…) But the threshold beyond which the surface is too rough to insure that no gloss component is captured is difficult to estimate, and there is no way to check it. Except for the special class of object described above, color and gloss are carried by mixed light components. Since color varies as a function of the viewing direction [5, 6, 7, 11, 12], intending to measure "one" color independently of gloss makes no sense. The problem becomes even more pregnant in the case of "effect materials", also called "goniochromatic materials", such as shot fabrics [13, 14], metal-pigmented paints and pearlescent coatings [15, 16, 17, 18]. A specific color characterization is needed, able to render important angular color variations.

The solution that we propose relies on the bidirectional reflectance distribution function (BRDF) of the object. This function specifies for each couple of incident and observation directions the ratio of the emitted radiance to the incident irradiance. It is measured using a gonioreflectometer [19, 20]. For each couple of directions, the measured reflectance spectrum is converted into CIEXYZ trichromatic values, then into CIELAB color coordinates by choosing a white reference. We recommend representing two additional points in the CIELAB color space, representing the color coordinates of a perfect white diffuser and the color of a perfect mirror. The two points show intuitively to which extend the considered specimen is rather specularly or diffusely reflecting.

The conversion of reflectance spectra into color coordinates is well established when the measuring geometry is fixed (fixed observation direction), but difficulties appear when observation direction varies. A very small solid angle is highly recommended if one desires acquiring the BRDF of glossy specimen with a satisfying accuracy. But since the color matching functions were established by the CIE in respect to cones of 2° and 10° half-angles (CIE1931 and CIE1964 respectively), it seems preferable to perform reflectance measurements with these solid angles. A solution would be to perform two measurements using first a very small solid angle to obtain the BRDF, and then a larger solid angle to calculate the reflectance factors and the color coordinates. Instead, we show that the second measurement is equivalent to applying an undersampling operation on the first one. Thus, a single high resolution measurement is needed and the color coordinates are calculated by considering precisely the solid angle defined by the CIE for colorimetry (2° or 10°).

The present paper is structured as follows: in section 2, we recall some essential radiometric definitions for the characterization of light reflection. Section 3 defines the color for two particular

cases: the Lambertian and the specular samples. Then, Section 4 presents the goniocolorimetric space and recaps the different steps for converting measured spectra into color coordinates. Section 5 illustrates the methodology with the example of a glossy and diffuse blue sample. Finally, Section 6 draws the conclusions.

2. *Radiometric definitions*

The angle-dependent reflection properties of an object are characterized by angular functions defined as ratios of radiometric quantities, e.g. the bidirectional reflectance distribution function (BRDF). This function can be measured using an instrument called gonioreflectometer which contains a movable collimated light source and a movable detector.

Let us consider a planar sample illuminated by a perfectly collimated light coming from a given direction (θ_i,φ_i). The sample reflects in direction (θ_r,φ_r) a radiance $L(\theta_i,\varphi_i,\theta_r,\varphi_r)$ defined as [21]:

$$L(\theta_i,\varphi_i,\theta_r,\varphi_r)=\frac{d^2\Phi_r(\theta_r,\varphi_r)}{dS\cos\theta_r d\omega_r} \tag{1}$$

where $d^2\Phi_r(\theta_r,\varphi_r)$ is the flux element reflected in the direction (θ_r,φ_r), dS is an elemental area on the sample and $d\omega_r=\sin\theta_r d\theta_r d\varphi_r$ is an infinitesimal solid angle in the considered direction.

Radiance factor and BRDF

The radiance factor, β, is defined as the ratio of the radiance $L(\theta_i,\varphi_i,\theta_r,\varphi_r)$ reflected by the sample to the radiance L_{ref} reflected by the perfect diffuser in the same illumination and observation conditions:

$$\beta(\theta_i,\varphi_i,\theta_r,\varphi_r)=\frac{L(\theta_i,\varphi_i,\theta_r,\varphi_r)}{L_{ref}} \tag{2}$$

The radiance coefficient q (in sr^{-1}) is now widely preferred to the radiance factor. It is defined as the ratio of the radiance $L(\theta_i,\varphi_i,\theta_r,\varphi_r)$ to the incident irradiance E_i:

$$q(\theta_i,\varphi_i,\theta_r,\varphi_r)=\frac{L(\theta_i,\varphi_i,\theta_r,\varphi_r)}{E_i} \tag{3}$$

However, in most setups, the incident irradiance is not measured directly but evaluated from a measurement on a perfect diffuser, i.e., a white diffusing sample obeying Lambert's law (appearing equally bright from all directions). The perfect white diffuser reflects a radiance L_{ref} proportional to the incident irradiance E_i [21]:

$$L_{ref}=E_i/\pi \tag{4}$$

This yields the following relation between radiance coefficient and radiance factor:

$$q(\theta_i,\varphi_i,\theta_r,\varphi_r)=\frac{\beta(\theta_i,\varphi_i,\theta_r,\varphi_r)}{\pi} \tag{5}$$

The BRDF is the function that describes the evolution of the radiance coefficient according to the directions of illumination and reflection.

Reflectance factor

In practice a detector does not measure a radiance but a flux in a finite solid angle. Since radiance factor and BRDF are defined in respect to an infinitesimal solid angle, they can not be measured directly. Hence, a reflectance factor R is defined as the ratio of the flux $\Delta\Phi_r(\theta_r,\varphi_r)$ reflected by the sample in the direction (θ_r,φ_r) and in a given solid angle to the flux $\Delta\Phi_{ref}(\theta_r,\varphi_r)$ reflected by the perfect diffuser exactly in the same illumination and observation conditions:

$$R(\theta_i,\varphi_i,\theta_r,\varphi_r)=\frac{\Delta\Phi_r(\theta_r,\varphi_r)}{\Delta\Phi_{ref}(\theta_r,\varphi_r)} \tag{6}$$

Let us calculate the flux $\Delta\Phi_r$ by assuming that the detector surface is perpendicular to the viewing direction and has a fixed area ΔS_d. The viewing solid angle $\Delta\Omega_d$, also fixed, is a cone centered on the detector surface normal. Through this cone, the detector observes an elliptical region of the sample, whose area varies with the cosine of the viewing angle θ_r. The observed area is generally different from the illuminated area, i.e. it is often wholly included within the illuminated area at small viewing angles and overpasses it at grazing angles. When calculating the measured flux, one should consider only the fraction of observed area that is illuminated, called the "emitting area" ΔS. This latter is a function of the observation direction (θ_r,φ_r).

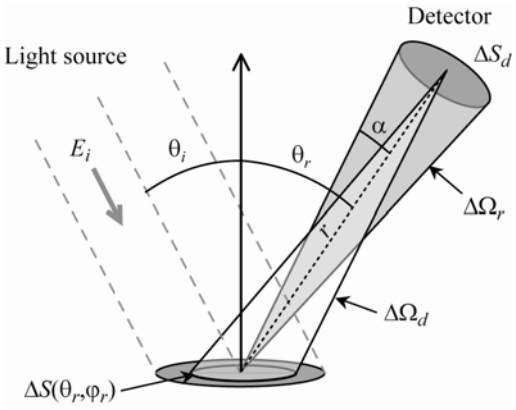

Figure 1: Geometry of a goniometric measurement.

The detector receives a collection of light rays, contained within the solid angle $\Delta\Omega_r$ based on the emitting area and subtended by its surface ΔS_d (Figure 1). Each light ray, propagating into a direction (θ'_r,φ'_r), corresponds to a radiance $L(\theta_i,\varphi_i,\theta'_r,\varphi'_r)$ defined in the same manner as in Eq.(1), and therefore to a flux element given by

$$d^2\Phi_r(\theta'_r,\varphi'_r)=L(\theta_i,\varphi_i,\theta'_r,\varphi'_r)\Delta S\cos\theta'_r\sin\theta'_r d\theta'_r d\phi'_r \tag{7}$$

The sum of the collected flux elements gives the measured flux. It may be expressed as a function of the radiance coefficient according to Eq. (3):

$$\Delta\Phi_r(\theta_r,\varphi_r)=E_i\Delta S\int_{(\theta'_r,\varphi'_r)\in\Delta\Omega_r} q(\theta_i,\varphi_i,\theta'_r,\varphi'_r)\cos\theta'_r\sin\theta'_r d\theta'_r d\varphi'_r \tag{8}$$

The flux reflected by the perfect diffuser is obtained with $q=1/\pi$

$$\Delta\Phi_{ref}(\theta_r,\varphi_r)=\frac{E_i\Delta S}{\pi}\int_{(\theta'_r,\varphi'_r)\in\Delta\Omega_r}\cos\theta'_r\sin\theta'_r d\theta'_r d\varphi'_r \tag{9}$$

From Eqs. (6), (8) and (9), one obtains the following expression for the reflectance factor

$$R(\theta_i,\varphi_i,\theta_r,\varphi_r)=\pi\frac{\int_{(\theta'_r,\varphi'_r)\in\Delta\Omega_r} q(\theta_i,\varphi_i,\theta'_r,\varphi'_r)\cos\theta'_r\sin\theta'_r d\theta'_r d\varphi'_r}{\int_{(\theta'_r,\varphi'_r)\in\Delta\Omega_r}\cos\theta'_r\sin\theta'_r d\theta'_r d\varphi'_r} \tag{10}$$

The integral of the denominator of Eq. (10) can be given a geometrical interpretation, described by Figure 2, leading to the following result:

$$\int_{(\theta'_r,\varphi'_r)\in\Delta\Omega_r}\cos\theta'_r\sin\theta'_r d\theta'_r d\varphi'_r=\frac{\Delta S_d}{r^2}\cos\theta_r \tag{11}$$

where r is the distance between the detector and the emitting surface.

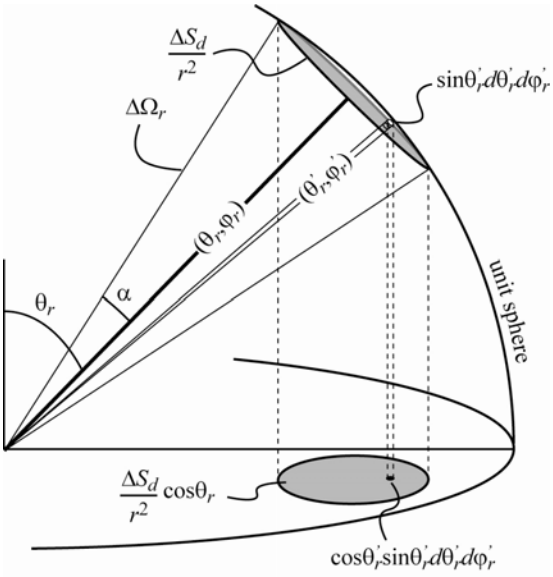

Figure 2: Interception of the solid angle $\Delta\Omega_r$ with the unit sphere and projection on the horizontal plane.

In the special case where the detector is located at $\theta_r=0°$, $\Delta\Omega_r$ is then called $\Delta\Omega_0$ and Eq. (11) can be written as:

$$\int_{(\theta'_r,\varphi'_r)\in\Delta\Omega_0}\cos\theta'_r\sin\theta'_r d\theta'_r d\varphi'_r=\frac{\Delta S_d}{r^2} \tag{12}$$

and since the detection was assumed to be in a cone of half-angle α, we also have:

$$\int_{(\theta'_r,\varphi'_r)\in\Delta\Omega_0}\cos\theta'_r\sin\theta'_r d\theta'_r d\varphi'_r=2\pi\int_{\theta'_r=0}^{\alpha}\cos\theta'_r\sin\theta'_r d\theta'_r=\pi\sin^2(\alpha). \tag{13}$$

Finally, according to Eqs. (10) to (13), we obtain

$$R(\theta_i,\varphi_i,\theta_r,\varphi_r)=\frac{\int_{(\theta'_r,\varphi'_r)\in\Delta\Omega_r} q(\theta_i,\varphi_i,\theta'_r,\varphi'_r)\cos\theta'_r\sin\theta'_r d\theta'_r d\varphi'_r}{\sin^2(\alpha)\cos\theta_r} \tag{14}$$

Reflectance

The reflectance ρ is the ratio of the total flux reflected by the sample Φ_r to the incident flux Φ_i:

$$\rho = \frac{\Phi_r}{\Phi_i} \tag{15}$$

The total flux element Φ_r reflected by the area element ΔS is given by the sum of the flux elements $d^2\Phi_r(\theta_r,\varphi_r)$ over the whole hemisphere. By extension of Eq. (8) to a hemispherical solid angle $(\Delta\Omega_r = 2\pi)$, we obtain

$$\Phi_r = E_i \Delta S \int_{\theta_r=0}^{\pi/2}\int_{\varphi_r=0}^{2\pi} q(\theta_i,\varphi_i,\theta_r,\varphi_r)\cos\theta_r \sin\theta_r d\theta_r d\varphi_r \tag{16}$$

As the incident flux Φ_i is equal to $E_i \Delta S_i$, where ΔS_i is the illuminated area, Eq. (15) becomes

$$\rho = \frac{\Delta S}{\Delta S_i}\int_{\theta_r=0}^{\pi/2}\int_{\varphi_r=0}^{2\pi} q(\theta_i,\varphi_i,\theta_r,\varphi_r)\cos\theta_r \sin\theta_r d\theta_r d\varphi_r \tag{17}$$

Reflectance can be measured with an integrating sphere, whose geometry usually ensures that $\Delta S = \Delta S_i$.

The reflectance factor tends towards the radiance factor when the solid angle becomes infinitesimal $(\Delta\Omega_r \to 0)$ and tends towards the reflectance when all the upper hemisphere is taken into account $(\Delta\Omega_r = 2\pi)$. Note that radiance factor and reflectance factor may reach values higher than 1, whereas reflectance is always lower than 1.

3. Color of Lambertian and specular samples

The colorimetric coordinates can be calculated from the reflectance factor and represented in 3-dimensional spaces defined by the CIE [1, 2, 3]. This calculation can be performed for any object but two types of samples are of particular importance when studying the angular colorimetric variations: the Lambertian and the specular samples.

3.1. CIEXYZ and CIELAB colorimetric spaces

The color of an object is represented by a set of three values deduced from the object reflectance factor. The CIEXYZ tristimulus values are obtained by multiplying the standardized illuminant radiance spectrum $S(\lambda)$, the object reflectance spectrum $R(\lambda)$ and each of the matching color functions $\bar{x}(\lambda)$, $\bar{y}(\lambda)$ and $\bar{z}(\lambda)$, then summing the resulting spectrum over the visible wavelength domain:

$$\begin{cases} X = k\sum_\lambda R(\lambda)S(\lambda)\bar{x}(\lambda) \\ Y = k\sum_\lambda R(\lambda)S(\lambda)\bar{y}(\lambda) \\ Z = k\sum_\lambda R(\lambda)S(\lambda)\bar{z}(\lambda) \end{cases} \tag{18}$$

where factor k is a normalization factor giving $Y = 100$ for the perfect white diffuser whose reflectance spectrum is $R(\lambda) = 1$, i.e.

$$k = \frac{100}{\sum_\lambda S(\lambda)\bar{y}(\lambda)}$$

The color matching functions $\bar{x}(\lambda)$, $\bar{y}(\lambda)$ and $\bar{z}(\lambda)$ have been determined for a fixed observation solid angle with half-angle α = 2° in the standard of CIE1931 and α = 10° in the standard of CIE1964.

The CIELAB color space, defined by the CIE in 1976, expresses three coordinates L^*, a^* and b^* derived from the CIEXYZ tristimulus values according to the following formulas:

$$\begin{cases} L^* = 116\, f\left(Y/Y_{ref}\right) - 16 \\ a^* = 500\left[f\left(X/X_{ref}\right) - f\left(Y/Y_{ref}\right)\right] \\ b^* = 200\left[f\left(Y/Y_{ref}\right) - f\left(Z/Z_{ref}\right)\right] \end{cases} \tag{19}$$

where

$$\begin{cases} f(A) = A^{1/3}, & A > \left(\dfrac{24}{116}\right)^3 \\ f(A) = \dfrac{841}{108}A + \dfrac{16}{116}, & A \le \left(\dfrac{24}{116}\right)^3 \text{ (Pauli's correction)} \end{cases} \tag{20}$$

and where X_{ref}, Y_{ref} and Z_{ref} are the CIEXYZ tristimulus values for a reference usually chosen as the perfect white diffuser, calculated for a constant spectrum $R(\lambda) = 1$.

3.2. Lambertian samples

A Lambertian sample is defined by a radiance factor β independent of the incident and observation directions. Its BRDF is constant, equal to β/π. By angular integration according to Eqs. (10) and (17), the reflectance factor R and the reflectance ρ are equal to β.

The Lambertian sample is said to be a "perfect white" when it absorbs no light, i.e. when $R(\lambda) = 1$. When it is itself chosen as the white reference, its CIELAB coordinates are $\left(L_w^*, a_w^*, b_w^*\right) = (100,0,0)$.

3.3. Specular samples

A sample is said to be "perfectly specular" when it reflects a collimated incident light into a single direction. Its reflectance $\rho(\theta_i)$ is a function of the illumination angle θ_i. According to Snell's laws, light is reflected at the angle θ_i and the azimuth angle $\varphi_i + \pi$. In the other directions, no light is reflected. The BRDF is given by the following bi-dimensional Dirac Delta function

$$q(\theta_i, \varphi_i, \theta_r, \varphi_r) = \rho(\theta_i) \frac{\delta(\theta_r - \theta_i)\delta(\varphi_i + \pi - \varphi_r)}{\cos\theta_i \sin\theta_i} \tag{21}$$

From Eq. (14), we obtain the following expression for the reflectance factor

$$R(\theta_r, \varphi_r) = \begin{cases} \dfrac{\rho(\theta_i)}{\sin^2\alpha \cos\theta_r}, & (\theta_i, \varphi_i + \pi) \in \Delta\Omega_r \\ 0 & \text{otherwise} \end{cases} \tag{22}$$

$\rho(\theta_i)$ can be obtained by angular integration according to Eq. (17) with $\Delta S = \Delta S_i$ and q given by Eq. (21), or by setting $\alpha = \pi/2$ and $\theta_r = 0$ into Eq. (22).

When $\rho(\theta_i) = 1$, the incident light is reflected without attenuation and the sample is called a "perfect mirror". Its reflectance factor, called γ, depends only on the geometry of the measuring system and is given by Eq. (22) with $R(\theta_i) = 1$ and $\theta_r = \theta_i$ in the specular direction:

$$\gamma = \frac{1}{\sin^2(\alpha)\cos\theta_i} \tag{23}$$

The color of the perfect mirror in the specular direction, in respect to the perfect white diffuser is given by the CIELAB coordinates $\left(L_m^*, a_m^*, b_m^*\right) = \left(\gamma^{1/3}116 - 16, 0, 0\right)$.

Both colors of the perfect white diffuser and the perfect mirror are located on the achromatic axis $\left(a^*, b^*\right) = (0,0)$. Since γ is larger than 1, the perfect mirror has a brighter color than the white diffuser, i.e. $L_m^* > L_w^*$. For example, if the perfect mirror is measured at $\theta_i = \theta_r = 0°$ and if $\alpha = 2°$, we have $\gamma \approx 821$ and the lightness of the perfect mirror is $L_m^* \approx 1070$. When $\alpha = 10°$, we have $\gamma \approx 33$ and $L_m^* \approx 357$.

4. Goniocolorimetry

We present in this section a methodology to define color variations with the viewing direction in the CIELAB colorimetric space as a function of viewing direction.

4.1. Choosing the viewing solid angle

Some objects have sharp angular reflection properties. For example, gloss is often focused on a precise direction. Measuring the BRDF of such objects requires a high angular precision, therefore a detector with small solid angle (cf. [8] for practical examples). The interpretation of gloss distinguishes the "specular gloss", related to the reflection in the specular direction, the "distinctness of image" related to the specular peak width, and the "gloss contrast" related to the ratio between the specular and the diffuse fluxes [22]. To measure gloss accurately, especially the distinctness of image, the viewing solid angle has to be smaller than the ocular acuity, which is estimated to 1 minute of arc.

Nevertheless, Eq. (23) indicates that a small value of α induces a very high value for the geometry factor γ and therefore an important source of imprecision in the colorimetric computations. For the color characterization, it is preferable to use a larger viewing solid angle and it looks judicious to select the one considered by the CIE when establishing the color matching functions, i.e. cones with half-angle α = 2° or 10°.

At first sight, the characterizations of gloss and of color look incompatible since they require different viewing solid angles, but in practice, it is sufficient to perform a single measurement at high angular resolution. This latter is subsequently undersampled for the color characterization, with a sampling angle of 2° or 10° to reproduce CIE's standard solid angles. This undersampling operation is at the base of so-called "abridged goniophotometry".

4.2. High angular resolution measurement

Let us measure the fluxes reflected by the object and by the perfect white diffuser using a very thin viewing solid angle, which may be written as $\delta\Omega_r = \sin\theta_r d\theta_r d\varphi_r$ where angles θ_r and φ_r denote the viewing direction. Since light rays flowing though it propagate nearly along the same direction $\left(\theta_r, \varphi_r\right)$, the integrals in Eq. (10) are reduced to a simpler form:

$$R\left(\theta_i, \varphi_i, \theta_r, \varphi_r\right) = \pi q\left(\theta_i, \varphi_i, \theta_r, \varphi_r\right) \tag{24}$$

Reflectance factor is therefore proportional to radiance coefficient in this case. Sève [8] recommends using a detector with viewing solid angle smaller than the ones usually found in glossmeters, e.g. with 0.5° half-angle solid angle, i.e. $\delta\Omega_r = 2.10^{-4}\, sr$.

4.3. Undersampling

We want to convert the measured spectral reflectance factor into color coordinates, i.e. into X, Y, Z tristimulus values, then into CIELAB coordinates. The color matching functions used for the computation of the tristimulus values have been established for a viewing solid angle $\Delta\Omega_r$ of either 2° or 10° half-angle. It looks therefore suitable to calculate color coordinates from spectra defined in respect to this solid angle. Obtaining these spectra is permitted by the following method.

Let us assume that spectral reflectance factor $R(\theta_i,\varphi_i,\theta_r,\varphi_r)$ is a continuous function of angles (θ_r,φ_r). If it was measured at discrete positions with high angular resolution, interpolation may be used. The radiance coefficient *q* can therefore be deduced from Eq. (24). Then, Eq. (10) yields a new reflectance factor $\rho'(\theta_i,\varphi_i,\theta_r,\varphi_r)$ that would be measured with the new viewing solid angle $\Delta\Omega_r$. This reflectance factor is consistent with color calculations.

In order to simplify the computations, in particular to avoid calculating the integrals of Eq. (10), we recommend a discrete approach based on a planar mapping of the BRDF. This mapping, already used by Elias [23] for the representation of BRDFs, is a Lambert azimuthal equal-area projection [24]. Every point P on the hemisphere, specified by its spherical coordinates (θ,φ), is mapped to a point P' of polar coordinates (r,φ) contained within a horizontal disk of radius $\sqrt{2}$ tangent to the hemisphere at the North pole N (Fig. 3). The azimuth coordinate φ is the same in the two coordinate systems. Coordinate *r*, which corresponds the distance NP, is given by

$$r = 2\sin(\theta/2)$$

Point P' is also be specified by the following Cartesian coordinates

$$\begin{aligned} u &= 2\sin(\theta/2)\cos\varphi \\ v &= 2\sin(\theta/2)\sin\varphi \end{aligned} \tag{25}$$

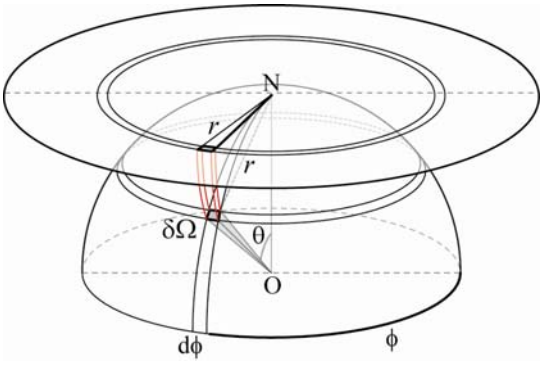

Figure 3: Mapping of the hemisphere onto a disk of radius $\sqrt{2}$ according to Lambert azimuthal equal-area projection applied at the North pole N.

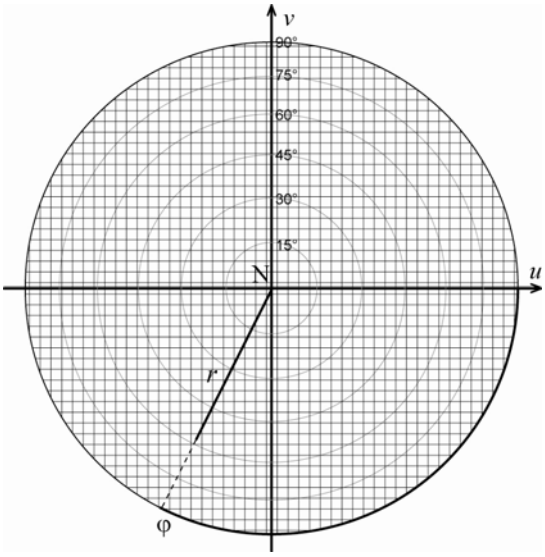

Figure 4: Sampled image of the BRDF projection disk where the pixel area corresponds to a viewing angle of 2° half-angle.

This mapping conserves areas. A portion of hemisphere with area *A* is mapped into a portion of disk with same area *A*. Conversely, the area of a disk element equals the area of the corresponding sphere element, thereby the value in steradian of the corresponding solid angle. By partitioning the disk according to a uniform grid (Fig. 4), one obtains a partition of the hemisphere where all the solid angles are equal.

Applying this mapping and this partitioning to the BRDF yields a multispectral image, i.e. a discrete image containing as many channels as wavelengths. Each pixel of the image corresponds to a same solid angle. Pixels with side *d* represent solid angles of d^2 steradians. When one desires considering a partition with larger solid angles, one can undersample the image in such manner that the area of the new pixels corresponds precisely to the desired solid angle. Classical resampling technics in image processing, e.g. bilinear resampling, may be used. In our case, we are interested in conical solid angle with half-angle $\alpha = 2°$ or 10°, whose area in steradian is $4\pi \sin^2(\alpha/2)$. The pixel side should therefore be

$$d = 2\sqrt{\pi}\sin(\alpha/2) \tag{26}$$

Note that the pixelization without overlapping in the (u,v) plane induces to choose a square base cone instead of the classical circular base cone. It is also possible to use a partition grid whose cells have a more circular shape, e.g. a hexagonal grid.

4.4. Color coordinates

Now, the undersampled multispectral image can be converted into CIELAB coordinates using Eqs. (18) and (19). Considering a given α value (2° or 10°), one obtains a 3-channel image where each pixel contains the three color coordinates, e.g. the L^*, a^* and b^* coordinates of the CIELAB color system. One may select a subset of pixels, corresponding to a subset of directions, and represent their associated color in the CIELAB space.

The geometry factor γ, given by Eq.(23), enables representing both the perfect white diffuser $(L_w^*, a_w^*, b_w^*) = (100,0,0)$ and the perfect mirror $(L_m^*, a_m^*, b_m^*) = (\gamma^{1/3}116 - 16,0,0)$ in the CIELAB space. Thanks to the undersampling procedure, the solid angle selected for color viewing is independent of

the one used for spectral measurements and the geometry factor γ, thereby the lightnesses of the perfect white diffuser and the perfect mirror, become independent of the experimental device.

4.5. Goniocolorimetry in 3 steps

The complete procedure to follow from flux measurement to CIELAB coordinates may be summarized by the three following steps:

1. Measurement: using a fixed collimated light and a gonioreflectometer with small solid angle, measure at high angle resolution the flux reflected by the sample to study and by the perfect white diffuser. Divide the measured flux of the sample by the measured flux of the perfect white diffuser. One obtains the reflectance factor of the sample.

2. Undersampling: choose a viewing solid angle for the color calculation (2° or 10°). Undersample the reflectance factor calculated in step 1, with a sampling rate corresponding to the selected viewing solid angle.

3. Colorimetry: calculate the color coordinates.

This ideal procedure must be modified in practice because, nowadays, the devices seldom achieve to obtain both a high angular resolution (e.g. $\Delta\Omega=10^{-4}$ sr) and a sufficient spectral resolution for colorimetric calculations (e.g. $\Delta\lambda$=5 nm). More sophisticated protocol should be proposed with sharp measurements for large BRDF variations, in particular around the specular direction, and more blur measurements elsewhere. In this last case, the second step should rather be called “resampling”. The operation consists in changing the initial non-uniform sampling to a uniform one. However, the same classical resampling technics adapted to an irregular grid can be applied.

5. Example

We propose to illustrate the methodology introduced above with the example of a glossy sample illuminated at normal incidence $(\theta_i = \varphi_i = 0)$. Its reflectance factor is supposed to be written as the superposition of a Lambertian diffuse component and a specular peak [25, 26]

$$R(\theta_r,\varphi_r) = R_d(\lambda) + \rho_s \frac{1}{2m^2\cos^3\xi}\exp\left(-\frac{\tan^2\xi}{2m^2}\right) \tag{27}$$

where R_d is the volume diffuse reflectance factor, ρ_s is the surface specular reflectance, m is the r.m.s. slope of the rough interface and ξ is the local incidence angle, i.e. half the angle between the illumination direction (θ_i,φ_i) and the observation direction (θ_r,φ_r) [27]. At normal incidence, we have $\xi = \theta_r/2$. The diffuse component R_d is a function of wavelength and corresponds to a blue color in the example whereas the reflectance ρ_s is assumed to be wavelength-independent (Figure 5).

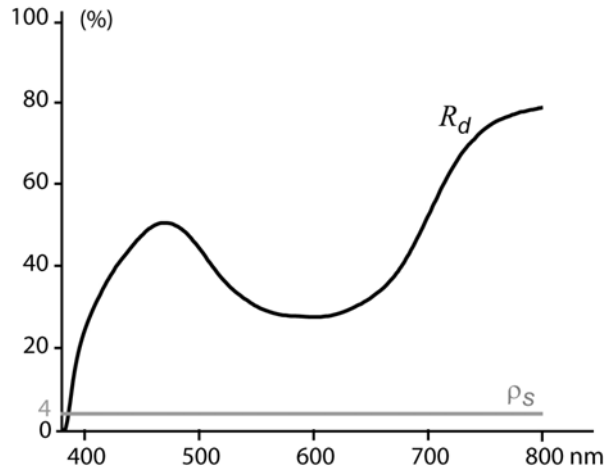

Figure 5: Spectral variations of the specular component ρ_s and of the diffuse component R_d for the reflectance factor simulation (Eq.(27)).

First, the flux reflected by the sample is acquired at a high angular resolution, i.e. with a small viewing solid angle $\delta\Omega_r$. Then we proceed to the undersampling operation, choosing a sampling solid angle with 2° or 10° half-angle. Since $\theta_i = 0°$, the geometry factor is accordingly $\gamma_{2°} = \sin^{-2}(2°)$ or $\gamma_{10°} = \sin^{-2}(10°)$. Figures 6 and 7 represent the reflectance factor before and after the two types of undersampling at the wavelength $\lambda = 700\,\text{nm}$ where $R_d = 0.5$, for a surface r.m.s. slope $m = 0.1$ and a surface reflectance $\rho_s = 0.04$. The reflectance factors are represented in Figure 6 in (u,v)-coordinates, derived from the (θ_r, φ_r)-coordinates according to transformation (25). In Figure 7, they are represented in the incident plane as a function of the viewing angle.

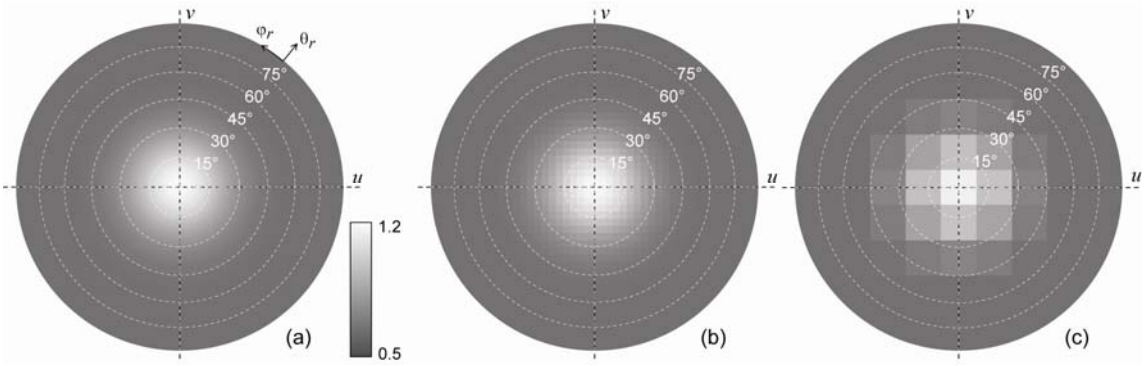

Figure 6: Reflectance factor at a normal incidence, simulated with Eq. (27) with m = 0.1, R_d = 0.5 and ρ_s = 0.04 and projected onto the (u,v)-plane according to the transformation defined by Eq. (25); (a) before undersampling, (b) after undersampling with α = 2° (grid spacing Δu = 0.049) and (c) after undersampling with α = 10° (grid spacing Δu = 0.247).

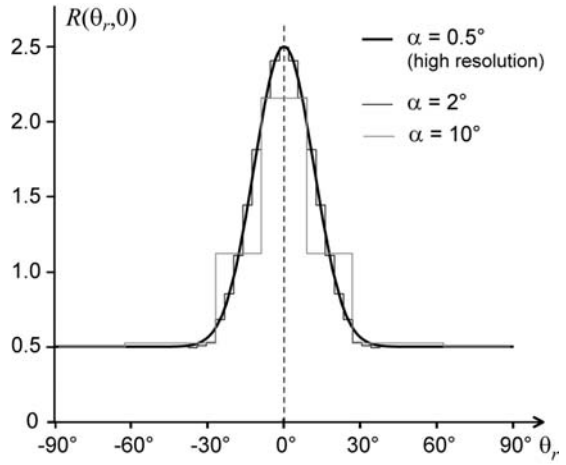

Figure 7: Profile of the reflectance factor plotted in Figure 6 along the *u*-axis, before and after each type of undersampling.

In the last step, the reflectance spectra calculated for each grid cell are converted into CIELAB coordinates, as well as the reflectance spectra of the perfect white diffuser and of the perfect mirror. All the corresponding points are placed in the goniocolorimetric CIELAB space. Note that lightness overpasses 100 when, in a given direction, more light is reflected by the sample than by the perfect white diffuser. For very glossy surfaces, lightness may vary over decades. Hence, it is preferable to represent lightness using a logarithm scale.

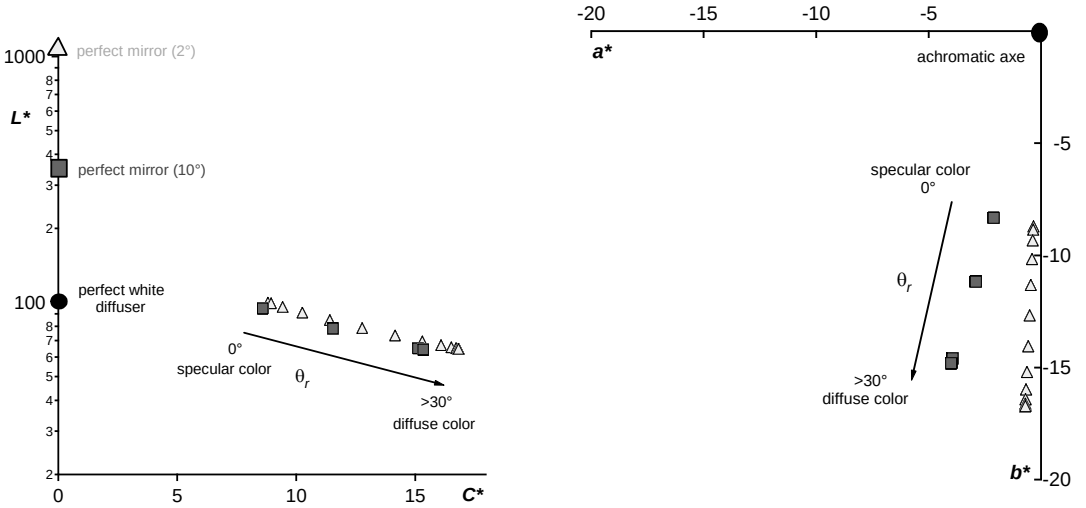

Figure 8: Color coordinates of a sample observed at different orientations θ_r represented in the (C^*,logL^*)-diagram (left) and the (a^*,b^*)-diagram (right) of the CIELAB space. Corresponding reflectance factors are simulated according to Eq. (27) at normal incidence, with $R_d(\lambda)$ and $\rho_s(\lambda)$ shown in Figure 5 and $m = 0.1$. The viewing solid angles are defined by $\alpha = 2°$ (△) and $\alpha = 10°$ (■).

Figure 8 shows the color variations obtained for viewing solid angles with 2° and 10° half-angle. We see that near the specular direction (θ_r tending to 0°), the color becomes paler (L^* increases and C^* decreases). This is the usual "goniocolorimetric behaviour" of glossy materials. It should be noticed that the two undersampling operations ($\alpha = 2°$ and $\alpha = 10°$) give different color coordinates for a

same direction due to different viewing solid angle over which the reflectance is averaged. At $\theta_r = 0°$, the CIELAB coordinates are respectively $(98.3,-0.3,-8.8)$ and $(94.6,-2.1,-8.3)$. However, these variations are small compared to the high lightness variation of the perfect mirror, detailed in Section 3.3 ($L^*_m = 1070.2$ for $\alpha = 2°$ and 356.7 for $\alpha = 10°$). The small coordinate differences (especially a hue angle difference) observed in the diffuse part when $\theta_r > 30°$, $(63.7, -0.7, -16.8)$ and $(64.5,-4.0,-14.8)$, are due to differences between the standard observer color matching functions defined by the CIE in 1931 and in 1964, and more precisely to the different foveal area stimulated by the viewing solid angle with $\alpha = 2°$ and $\alpha = 10°$.

6. Conclusion

The goniocolorimetric space introduced in this paper is a CIELAB color space where the colors of a same object viewed at different angles are represented. Since the amount of light reflected in the specular direction may be much higher than the amount of light reflected by the perfect white diffuser used as reference, lightness may overpass 100. The highest lightness value is obtained from a perfect mirror viewed in the specular direction. This value is systematically represented in the goniocolorimetric space in such manner to have a scale of gloss, i.e. a scale for "reading" high lightness values. As an advantage of the proposed methodology, color coordinates are calculated by considering the viewing solid angles considered by the CIE when establishing the color matching functions, i.e. solid angles with 2° or 10° half-angle. This viewing solid angle is introduced while converting the BRDF, measured with a thinner solid angle, into a multispectral planar image whose pixel size is directly related to the considered solid angle. This mathematical procedure allows the independence of the color calculation from the measurement setup.

The method proposed here needs to be tested on a wide range of samples in order to evaluate its limitations. At first sight, it is difficult to evaluate the pertinence of the color coordinates computed in directions where the spectral BRDF varies very strongly within the considered solid angle. This question might necessitate a wide experiment based on visual testing. On the other hand, the connection between the BRDF (cone issued from the surface) and the visual field (cone issued from the detector) is not as simple as supposed in our paper. When the solid angle is very small, the radiance invariance principle ensures that the radiance emitted by the surface and the one received by the detector are equal. But when a larger solid angle is considered, the texture or the curvature of the surface may have an influence on the perception. It appears that our work is limited to samples whose surface is rather homogenous and plane. The case of objects presenting a strongly textured aspect or a non negligible radius of curvature is therefore beyond the scope of the present study and represents a challenge for further investigation.

The notion of goniocolorimetric space was presented for reflectance, but it can be extended in a straightforward manner to transmittance. The only difference concerns the reference samples. For direct transmission (the equivalent for specular in reflection), the reference is the direct measurement of the incident light without sample (in practice, this direct measurement is also often used as reference for specular reflection measurements instead of perfect mirror). A Lambertian reference for diffuse transmission measurements is not usual. In this case, the perfect white diffuser, reference for diffuse reflection measurements, can also be used as reference for diffuse transmission measurements.

References

1. *Colorimetry*, 3rd edition, Technical Report CIE 15:2004.

2. Wyszecki G, Stiles WS. Color science: Concepts and methods, quantitative Data and Formulae. 2nd ed. New York: Wiley Interscience Publication; 1982.

3. Sharma G. Color fundamentals for digital imaging. In: Digital Color Imaging Handbook, Ed. G. Sharma, CRC Press; 2003. p 30-36.

4. Oleari C. Colorimetry in Optical Coating. Proc of SPIE 2005;5963:5-15.

5. Baba G, Suzuki K. Gonio-spectrophotometric analysis of white and chromatic reference materials. Analytica Chimica Acta 1999;380:173-182.

6. Mikula M, Ceppan M, Vasko K. Gloss and Goniocolorimetry of Printed Materials. Col. Res. and appl. 2003;28:335-342.

7. Westlund HB, Meyer GW. Applying appearance standards to light reflection models. ACM SIGGRAPH Conference on computer graphics 2001;501-510.

8. Seve R. Problems connected with the concept of gloss, Col. Res. and Appl. 1993;18:241-252.

9. Obein G, Knoblauch K, Viénot F. Difference scaling of gloss: Nonlinearity, binocularity, and constancy. Journal of Vision 2004;4:711-720.

10. Ji W, Pointer MR, Luo RM, Dakin J. Gloss as an aspect of the measurement of appearance. JOSA A

11. Simonot L, Elias M. Color change due to surface state modification. Col. Res. and appl. 2003;28:45-49.

12. Simonot L, Elias M. Color change due to a varnish layer. Col. Res. and appl. 2004;29:196-204.

2006;23;22-33.

13. Kuehni RG. Cangiante : a fabric and a coloristic device in the art of the renaissance. Col. Res. and appl. 1996;21:326-330.

14. Lu R, Koenderink JJ, Kappers AML. Optical properties (bidirectional reflectance distribution function) of shot fabric. Applied Optics. 2000;39:5785-5795.

15. McCamy CS. Observation and measurement of the appearance of metallic materials. Part I. Macro appearance. Col. Res. and appl. 1996;21:292-303.

16. McCamy CS. Observation and measurement of the appearance of metallic materials. Part II. Micro appearance. Col. Res. and appl. 1998;23:362-373.

17. Nadal ME, Early EA. Color Measurements for Pearlescent Coatings. Col. Res. and appl. 2004;29:38-42.

18 Ershov S, Kolchin K, Myszkowski K. Rendering appearance based on paint-composition modeling. Computer Graphics Forum 2001;20:227-238.

19. Obein G, Bousquet R, Nadal ME. New NIST reference goniospectrometer. Proc. SPIE 2005;5880:241-250.

20. Hünerhoff D, Grusemann U, Höpe A. New robot-based gonioreflectometer for measuring spectral diffuse reflection. Metrologia 2006;43:S11–S16.

21. McCluney WR. Introduction to radiometry and photometry. Boston: Artech House; 1994. p 7-19.

22. Hunter RS. The measurement of appearance. New York: John Wiley & sons; 1987.

23. Elias M, Elias G. Radiative transfer in inhomogeneous stratified scattering media with use of the auxiliary function method. JOSA A 2004;21:580-589.

24. Snyder J P. Map Projections – A Working Manual. U. S. Geological Survey Professional Paper 1395. Washington, DC: U. S. Government Printing Office; 1987. p 182-190.

25. Torrance KM, Sparrow EM. Theory for Off-Specular Reflection from Roughened Surfaces. JOSA A 1967;9:1105-1114.

26. Hébert M, Hersch RD. Extending the Clapper-Yule model to rough printing support. JOSA A 2005;22:1962-1967.

27. Simonot L, Obein G. Geometrical considerations in analyzing isotropic or anisotropic surface reflections. Applied optics 2007;46:2615-2623.